



Fabrication of Ag-Pd Concave Nanocrystals through Facet-Selective Oxidation of Ag Atoms

Journal:	<i>Nanoscale</i>
Manuscript ID	NR-ART-02-2019-001250.R1
Article Type:	Paper
Date Submitted by the Author:	14-Mar-2019
Complete List of Authors:	Luo, Zheyu; Georgia Institute of Technology, Materials Science and Engineering Ahn, Jaewan; Georgia Institute of Technology, Materials Science and Engineering Qin, Dong; Georgia Institute of Technology, Materials Science and Engineering

Fabrication of Ag-Pd Concave Nanocrystals through Facet-Selective Oxidation of Ag Atoms

*Zheyu Luo, Jaewan Ahn, and Dong Qin**

School of Materials Science and Engineering, Georgia Institute of Technology, Atlanta, Georgia 30332, United States

*Corresponding author: dong.qin@mse.gatech.edu

ABSTRACT

We report the fabrication of Ag-Pd concave nanocrystals by introducing the Pd(II) precursor into an aqueous suspension of Ag nanocubes in the presence of cetyltrimethylammonium chloride (CTAC) under ambient conditions. Different from the previously reported work that involved the oxidation of Ag and deposition of Pd at random sites on the surface for the generation of Ag-Pd hollow nanocrystals, we demonstrate that the Cl^- ions from CTAC can confine the oxidation of Ag atoms to the side faces of a nanocube while the resultant Pd atoms are deposited on the edges in an orthogonal manner. By controlling the amount of the Pd(II) precursor involved in a synthesis, we can transform Ag nanocubes into Ag-Pd nanocrystals with different degrees of concaveness for the side faces and controllable Pd contents. We characterize the outermost layer of concave surfaces for the as-obtained Ag-Pd nanocrystals by surface-enhanced Raman scattering (SERS) through the use of an isocyanide probe. This facile approach would enable the fabrication of Ag-based concave nanocrystals for applications in plasmonics and catalysis.

Introduction

Silver nanocrystals embrace fascinating plasmonic properties that are essential to an array of applications related to localized surface plasmon resonance (LSPR),¹⁻⁵ sensing,^{6,7} and surface-enhanced Raman scattering (SERS).⁸⁻¹² However, they are limited in use for catalysis because Ag only exhibits strong activity toward oxidation reactions,^{13,14} such as epoxidation reaction, rather than reduction reactions. In principle, one can decorate the surface of Ag nanocrystals with Pd for the generation of Ag-Pd bimetallic nanocrystals to enhance the catalytic capability of Ag toward chemical reduction because Pd can catalyze a large number of reduction reactions such as hydrogenation. More significantly, such bimetallic nanocrystals with the integration of SERS and catalytic activities, arising from Ag and Pd, respectively, can also serve as a dual-functional system for investigating catalytic reactions *in situ* through SERS fingerprinting.¹⁵⁻¹⁷

There are three documented strategies for the synthesis of Ag-Pd nanocrystals. The first approach uses the galvanic replacement reaction between Ag nanocrystals and Na_2PdCl_4 in an aqueous solution for the generation of Ag-Pd bimetallic hollow nanostructures with tunable compositions and catalytic properties.¹⁸⁻²⁰ Because one Pd atom is generated at the expense of two Ag atoms, galvanic replacement will result in a significant loss of Ag and thus deterioration in SERS activity for the resultant nanocrystals. The second strategy couples the galvanic replacement reaction with chemical reduction by introducing an additional reducing agent for the synthesis of Ag-Pd hollow nanostructures.²¹ In this case, the Ag(I) ions dissolved from the original Ag nanocrystals through galvanic replacement can be reduced to Ag atoms for their co-deposition with the Pd atoms onto the nanocrystals. Although the hollow nanostructures can exhibit stronger SERS activity, it is difficult to confine the deposition of Pd at specific sites on the surface of the nanocrystals because the galvanic replacement reaction tends to occur at random locations. The third strategy eliminates the galvanic replacement reaction by co-reducing AgNO_3 and Na_2PdCl_4 with a strong reductant such as ascorbic acid (H_2Asc) to generate Ag and Pd atoms for their concomitant deposition on the edges of Ag nanocubes for the generation of Ag@Ag-Pd core-frame nanocubes in a manner similar to seeded growth.^{22,23} In this approach, Pd atoms can be confined to the edges of the nanocubes, but they are alloyed with the co-deposited Ag atoms, leading to compromised catalytic activities. Taken together, it remains a challenging task to fabricate Ag-Pd nanocrystals with concave side faces, together with an outermost surface covered by Pd atoms. As documented in the literature, the metal nanocrystals with concave surfaces serve as a platform for

many applications that include plasmonics, surface-enhanced Raman spectroscopy, and catalysis.²⁴⁻³⁰

Herein we report the fabrication of Ag-Pd bimetallic concave nanocrystals through a site-selective galvanic replacement reaction. In a typical process, we dispersed Ag nanocubes in an aqueous solution in the presence of cetyltrimethylammonium chloride (CTAC) and then introduce a mixture of Na₂PdCl₄ and CTAC solutions through multiple steps of injection under ambient conditions. The CTAC is able to facilitate galvanic replacement reaction in a site-controlled manner, together with its role as a colloidal stabilizer. Specifically, the Cl⁻ ions from CTAC can selectively cap the {100} facets on Ag nanocubes,³¹ making the side faces more vulnerable to the oxidation of Ag for the release of Ag(I) ions into the reaction solution. When an excessive amount of Cl⁻ ions is involved, most of dissolved Ag(I) ions will form AgCl₂⁻ in a soluble form to remain in the solution.³² On the other hand, when Na₂PdCl₄ is prepared in the presence of CTAC, the Cl⁻ ions can strongly inhibit the hydrolysis of PdCl₄²⁻ in an aqueous solution,³³ creating a stable Pd(II) precursor in the form of PdCl₄²⁻ to react with the Ag nanocubes and thus direct the reaction in a controllable and reproducible manner. By simply controlling the local concentration of the Pd(II) precursor and the amount of the Pd(II) precursor involved in the galvanic replacement reaction, we demonstrate the ability to selectively remove Ag atoms from the side faces of a nanocube for the concomitant deposition of Pd on the edges in an orthogonal manner, transforming Ag nanocubes into Ag-Pd nanocrystals with concave side faces. We also use an isocyanide molecule to characterize the outermost layer of concave surfaces for the as-prepared Ag-Pd nanocrystals by SERS. It is found that the outermost surface is composed of both Pd and Ag atoms when Ag nanocubes are decorated with 0.4 wt.% Pd. As the Pd content is increased to 0.8 wt.%, we observe a Pd-dominated outermost surface for the bimetallic nanocrystals. Collectively, we believe that this facile synthesis allows the generation of Ag-based concave nanocrystals with a second metal being deposited on their surfaces with controls in composition.

Experimental

Chemicals and materials

Ethylene glycol (EG) was ordered from J.T. Baker. Sodium hydrosulfide hydrate (NaSH·xH₂O), aqueous hydrochloric acid (HCl, 37%), poly(vinylpyrrolidone) (PVP) with an average molecular weight of 29000 (PVP-29k) or 55000 (PVP-55k), silver trifluoroacetate (CF₃COOAg, ≥99.99%

trace metal basis), aqueous cetyltrimethylammonium chloride (CTAC, 25 wt.%), sodium tetrachloropalladate(II) (Na_2PdCl_4 , $\geq 99.99\%$ trace metal basis), iron(III) nitrate nonahydrate ($\text{Fe}(\text{NO}_3)_3 \cdot 9\text{H}_2\text{O}$, $\geq 98\%$), aqueous nitric acid (HNO_3 , 70%), 2,6-dimethylphenyl isocyanide, (2,6-DMPI, $\geq 98\%$), and ethanol ($\text{CH}_3\text{CH}_2\text{OH}$, 200 proof) were all purchased from Sigma-Aldrich. Acetone (HPLC grade, 99.5+%) was obtained from Alfa Aesar. All the chemicals were used as received. The deionized (DI) water used in all experiments had a resistivity of 18.2 $\text{M}\Omega\text{-cm}$ at room temperature.

Synthesis of Ag nanocubes

We prepared the Ag nanocubes with an average edge length of 40.1 ± 2.4 nm using the polyol method.³⁴ We washed the as-obtained Ag nanocubes with acetone and water once each and then re-dispersed them in water for further use.

Preparation of aqueous Na_2PdCl_4 solution

We first dissolved Na_2PdCl_4 in water for 20 min to obtain aqueous Na_2PdCl_4 solution with a molar concentration of 1.0 mM. We then diluted the solution with water to attain a final concentration of 0.06 mM.

Preparation of the Pd(II) precursor solution

We dissolved Na_2PdCl_4 in water at room temperature for 20 min to obtain aqueous Na_2PdCl_4 solution with a concentration of 1.0 mM. We then diluted this solution with 100 mM aqueous CTAC solution to attain the Pd(II) precursor solution with a final concentration of 0.06 mM.

Synthesis of Ag-Pd nanocrystals in the presence of CTAC

Firstly, we added 2 mL of aqueous CTAC (100 mM), 1 mL of water, and 30 μL of the aqueous suspension of Ag nanocubes (approximately 1.03×10^{11} particles in total) to a glass vial in sequence under magnetic stirring at room temperature. Secondly, we introduced different volumes of the Pd(II) precursor solution (0.06 mM) into the reaction system through multiple steps of injection. Typically, we started with two consecutive steps of injection, with 0.05 mL per step, followed by additional steps of injection with a volume of 0.1 mL per step till 0.4 mL was attained. Beyond 0.4 mL, we switched to injection with 0.2 mL per step till the desired volume was achieved.

We also allowed the reaction to proceed for 30 min after each step of injection. Finally, we collected the solid products through centrifugation at 7000 rpm for 10 min, washed with water, and then re-collected through centrifugation at 5000 rpm for 10 min before they were re-dispersed in water for further use.

Etching of Ag from the Ag-Pd nanocrystals

We mixed aqueous $\text{Fe}(\text{NO}_3)_3$ (1 mM) with aqueous HNO_3 (3 mM) at 1:1 volume ratio to obtain an etching solution. In a typical etching process, we drop-casted the as-prepared Ag-Pd nanocrystals on a TEM grid. Upon drying, we immersed the TEM grid to 1 mL of the etching solution and incubated at room temperature for 1 h. The TEM grid was rinsed with water and then dried in the air prior to TEM characterization.

Synthesis of Ag-Pd nanocrystals in the presence of PVP

We introduced 2 mL of PVP-29k (1 mM), 1 mL of water, and 30 μL of the aqueous suspension of Ag nanocubes to a glass vial under magnetic stirring at room temperature. Next, we injected different volumes of aqueous Na_2PdCl_4 into the reaction system using a pipette in one shot. After 60 min, we collected the solid products by centrifugation at 14000 rpm for 10 min, washed the solids twice with water, and collected solids again through centrifugation at 14000 rpm before they were re-dispersed in water for further use.

Instrumentation and characterization

We used a Cary 50 spectrophotometer (Agilent Technologies, Santa Clara, CA) to record UV-vis spectra. We used an Eppendorf 5430 centrifuge (Eppendorf North America, Hauppauge, NY) to separate solid products from the supernatant. We used a Hitachi HT7700 microscope (Tokyo, Japan) operated at 120 kV to acquire TEM images. We used a Hitachi HD2700 C_s -corrected microscope operated at 200 kV to capture HAADF-STEM images. We performed elemental mapping of nanocrystals with an energy-dispersive X-ray spectroscopy (EDS) detector on the HD2700 microscope. We analyzed the Ag and Pd contents using a NexION 300Q ICP-MS (PerkinElmer, Waltham, MA). We collected the SERS spectra using a Renishaw inVia Raman Spectrometer (Wotton-under-Edge, UK) integrated with a Leica microscope (Wetzlar, Germany). We used a Thermo K-Alpha X ray photoelectron spectrometer (XPS, Thermo Fisher Scientific,

Waltham, MA) to record XPS spectra.

SERS characterization Ag nanocubes and Ag-Pd nanocrystals with 2,6-DMPI

We incubated the as-obtained nanocrystals in the 2,6-DMPI ethanol solution (10^{-5} M) for 1 h. Next, we collected nanoparticles through centrifugation at 3000 rpm and washed with water once before they were re-dispersed in 200 μ L of water for SERS measurements. We fabricated a sample cell by punching a small hole to accommodate 25 μ L of liquid sample in a polydimethylsiloxane (PDMS) block. After the PDMS was attached to a glass slide, we loaded the sample solution and then placed a glass coverslip of 170 μ m thickness on top of the PDMS to prevent solvent evaporation. We collected the SERS spectra in solution phase with a 100 \times objective at the excitation wavelength at 532 nm, together with a data collection time of 10 s at 100% laser power of 50 mW laser power.

Results and discussion

We started with the synthesis of Ag nanocubes having an average edge length of 40.1 ± 2.4 nm (Figure S1). We then dispersed them in an aqueous solution containing CTAC before the Pd(II) precursor solution was introduced through multiple steps of injections under ambient conditions (see details in the experimental section). It is worth emphasizing that the Pd(II) precursor solution was prepared by diluting aqueous Na_2PdCl_4 with aqueous CTAC to obtain a solution containing 0.06 mM Pd(II).^{33,35} We used UV-vis spectroscopy to characterize the as-prepared Pd(II) precursor solution. As shown in Figure S2A, the two peaks located at 225 and 285 nm can be assigned to the PdCl_4^{2-} species, ruling out the possibility of hydrolysis.³⁵ Additionally, we noticed that there was essentially no change to these two peaks when the solution was left under ambient conditions for 10 days when the vial of solution was covered by aluminum foil. These observations confirmed that the Cl^- ions from CTAC could shift the hydrolysis reaction of PdCl_4^{2-} to the left side, making it possible to keep PdCl_4^{2-} as a stable form in the aqueous solution. For comparison, Figure S2B shows the UV-vis spectra recorded from an aqueous solution of Na_2PdCl_4 (0.06 mM, but in the absence of CTAC) as a function of time. We noticed that the two peaks associated with PdCl_4^{2-} could no longer be observed and the spectra changed constantly in the span of 60 min, suggesting the hydrolysis of PdCl_4^{2-} to produce other species such as $\text{PdCl}_x(\text{H}_2\text{O})_{4-x}^{2-x}$ ($x = 1, 2, 3$) and even $\text{Pd}(\text{OH})_2$.³⁶

We used transmission electron microscopy (TEM) to characterize the solid products obtained after the Ag nanocubes had reacted with different volumes of the Pd(II) solution in the presence of CTAC. At 0.05 mL, Figure 1A shows that the morphology of the original Ag nanocubes was essentially retained. At 0.1 mL, Figure 1B indicates the appearance of cavities on the side faces. As the volume was further increased to 0.2, 0.3, and 0.4 mL, Figure 1, C-E, shows the formation of nanocrystals with more significantly concaved side faces. To confirm the deposition of Pd, we used aqueous $\text{Fe}(\text{NO}_3)_3/\text{HNO}_3$ to selectively remove Ag but not Pd through chemical etching. Figure S3, A-D, shows TEM images of the nanostructures derived from the etching of samples shown in Figure 2, B-E, from which we observed the formation of broken nanoframes. These results suggest that the limited number of Pd atoms were initially deposited on the edges of the nanocubes, consistent with our previous findings.^{22,23} We also used UV-vis spectroscopy to monitor the changes to the LSPR properties of the Ag nanocubes. Figure 1F shows that the major LSPR peak of the Ag nanocubes was progressively red-shifted from 434 to 443, 463, 511, 559, and 600 nm at injection volumes of 0.05, 0.1, 0.2, 0.3, and 0.4 mL, respectively. The cavities on the side faces of the nanocrystals were responsible for the changes in LSPR peak position while the loss of Ag from the nanocrystals could account for the decrease in peak intensity.

We also investigated the reaction between the Ag nanocubes and the Pd(II) precursor solution at 0.6, 0.8, and 1.0 mL, respectively. As shown in Figure S4, A-C, we observed the generation of hollow nanocrystals and nanoframes with rough ridges, indicating that the galvanic replacement reaction progressed continuously to carve out more Ag atoms from the side faces, accompanied by the deposition of Pd atoms on the edges and corners. During this transformation, the LSPR peaks of the resultant nanostructures were further red-shifted to 684, 784, 944 nm, respectively, together with a decrease in peak intensity (Figure S4D). These results suggest that it is critical to control the amount of the Pd(II) precursor involved in a synthesis for the transformation of Ag nanocubes into Ag-Pd concave nanocrystals rather than hollow nanostructures and nanoframes through galvanic replacement reaction.

To reveal the detailed structure and morphology of the concave nanocrystals, we used aberration-corrected high-angle annular dark-field scanning TEM (HAADF-STEM) to characterize a sample prepared with 0.4 mL of the Pd(II) precursor solution. Figure 2A shows a HAADF-STEM image taken from a nanoparticle that was tilted along the [001] zone axis. Figure 2, B and C, shows two atomic-resolution HAADF-STEM images collected from a zoomed region

located on one of the side faces. By focusing the electron beam on top of the particle, we resolved the columns of atoms located on the $\{100\}$ facets (Figure 2B). By simply refocusing the electron beam further away from the top to the bottom of the particle, we identified those atoms situated on the backside of the $\{100\}$ facets (Figure 2C). These results confirm the preferential carving of Ag from the side faces of a nanocube through galvanic replacement reaction. We also performed HAADF-STEM and EDS analyses on another sample prepared with 0.4 mL of the Pd(II) precursor. Figure 2, D-F, shows the spatial distributions of Ag, Pd, and Cl with a particle, respectively. It was found that Ag and Pd were distributed across the entire surface of the particle. This result suggests the diffusion of Pd adatoms from edges to other surfaces. The presence of Cl signal supported our argument that CTAC could bind to Ag nanocubes. We further characterized the same sample by EDS line scanning analysis with two orientations for the particle. As shown in Figure 3, A and B, the line profiles of Ag and Pd on a particle confirm the co-location of Ag and Pd at different sites of the concave nanocrystal.

Based on the results presented in Figures 1-3, we proposed a reaction pathway to account for the transformation of Ag nanocubes into Ag-Pd concave nanocrystals in the presence of CTAC through galvanic replacement reaction (Figure 4). We argue that the Cl^- ions derived from CTAC can preferentially bind to the $\{100\}$ facets on Ag nanocubes, making these sites more susceptible to oxidation and etching. Under this circumstance, Ag atoms are oxidized into Ag(I) ions for their release into the reaction solution, leading to the formation of cavities on the side faces of a Ag nanocube, consistent with our previous finding.³⁷ Most of these dissolved Ag(I) ions would form AgCl_2^- complex to stay in the soluble form when an excess amount of Cl^- ions is involved in the synthesis.³² On the other hand, Pd atoms are generated through the galvanic replacement reaction between the Pd(II) precursor and Ag for their preferential deposition on the edges, the $\{110\}$ facets with the highest energy, followed by diffusion across the surface to other regions. By simply changing the amount of the Pd(II) precursor solution involved in a synthesis, it is feasible to carve Ag atoms from the side faces of nanocubes selectively for their transformation into Ag-Pd concave nanocrystals with different Pd contents.

It is worth mentioning that the introduction of the Pd(II) precursor solution through multiple steps of injection rather than in one shot also plays an essential role in exquisitely controlling the local concentration of Pd(II) for the oxidation of Ag on the side faces and subsequent deposition of Pd on the edges of nanocubes. In fact, we performed two control experiments by introducing

the Pd(II) precursor solution using one-shot injection. At 0.2 and 0.4 mL, Figure S5, A and B, shows the resultant nanostructures accordingly. Although there was no major difference in morphology for the samples shown in Figure S5A and Figure 1C at an injection volume of 0.2 mL, we identified the formation of hollow nanostructures at 0.4 mL. These results suggest that the galvanic replacement reaction would proceed more rapidly at a high local concentration, leading to the transformation of Ag nanocubes into nanocrystals with different morphologies.

To further confirm the critical role of CTAC in the synthesis of Ag-Pd concave nanocrystals, we performed another set of experiments by revising the standard protocol. Firstly, we replaced CTAC with PVP as a colloidal stabilizer. Secondly, we prepared 0.06 mM aqueous Na_2PdCl_4 solution by eliminating the use of CTAC. Thirdly, we injected different volumes of the Pd(II) precursor solution in one shot to replace the multiple steps of injection to avoid hydrolysis. Figure S6, A and B, shows TEM images of the solid products obtained with the Na_2PdCl_4 solution at 0.2 and 0.4, mL, respectively, indicating that the morphology of the nanocrystals remained essentially the same as that of the original Ag nanocubes (see Figure S1). As the injection volume of the Na_2PdCl_4 solution was increased to 0.6, 0.8, and 1.0 mL, Figure S6, C-E, shows the emergence of random pits on the side faces of nanocubes, completely different from the hollow nanoparticles obtained by reacting the Ag nanocubes with the same volumes of the Pd(II) solution in the presence of CTAC (see Figure S4, A-C). Figure S6F shows UV-vis spectra of the Ag nanocubes before and after they had reacted with different volumes of Na_2PdCl_4 solution in presence of PVP. We noticed that the LSPR peak of the Ag nanocubes only shifted from 431 to 434, 439, 445, 456, and 457 nm as the volume of Na_2PdCl_4 solution was increased to 1.0 mL, which is completely different from those shown in Figures, 1F and S4D. Altogether, our results indicate that CTAC could enable site-selective galvanic replacement reaction to transform Ag nanocubes into Ag-Pd concave nanocrystals while PVP could only lead to the formation of random pits on the surface.

To understand the mechanistic details behind the synthesis, we used inductively coupled plasma mass spectrometry (ICP-MS) to quantify both the Pd and Ag contents in the Ag-Pd nanocrystals (solids) and the reaction solution (supernatant) after the Ag nanocubes had reacted with different volumes of the Pd(II) precursor solution. Specifically, we collected both solids and supernatants through centrifugation from each product for ICP-MS analyses. We performed the measurements twice and the results are summarized in Tables S1 and S2. By plotting the average amounts of the Pd in the solids and the Ag(I) in the supernatant as a function of volume of Pd(II)

precursor, Figure 5 shows linear increase for both Pd in solids and Ag(I) in supernatant with two slopes at values of 5.89 and 15.81, respectively. As such, our ICP-MS analyses give an atomic ratio of Pd to Ag(I) at about 1:2.7 that is higher than 1:2 by assuming that one Pd atom is produced at the expense of two Ag atoms through galvanic replacement reaction. We argue that such discrepancy could arise from possibility of having some particles remained in the supernatant after a centrifugation process to prepare the samples of solids and supernatant. In fact, the curve fitting of Ag(I) shows the intercept at 3.67 μg , supporting our argument on the presence of Ag nanocubes in the supernatant. By using the ICP-MS data of Pd and Ag in solids, we also calculated the Pd wt.% for Ag-Pd nanocrystals at 0.8%, 1.6%, 2.2%, and 2.8% after Ag nanocubes had reacted with 0.1, 0.2, 0.3, and 0.4 mL of Pd(II) precursor solution, respectively (Table S3). Because it was difficult to directly measure the Pd content of nanoparticles prepared by 0.05 mL of Pd(II) solution, we estimated the value of these nanocrystals at 0.4 wt.% Pd by using the data point of 0.1 mL. It is also worth mentioning that the conversion of the added Pd(II) precursor solution to Pd in the solids was about 86% (see Table S3). We also used the XPS to analyze the Pd deposited on the Ag nanocubes. Figure S7 shows the spectra recorded from three samples prepared by 0.05, 0.2, and 0.4 mL of Pd(II) precursor, respectively. It was found that the amount of Pd increased with the injection volume, consistent with ICP-MS results. Additionally, we noticed that the gaps between the $3d_{5/2}$ and $3d_{3/2}$ peaks of Ag ($\Delta=6.0$ eV) and those between the $3d_{3/2}$ and $3d_{5/2}$ peaks of Pd ($\Delta=5.3$ eV) are exactly the same as the values for zero-valent Ag and Pd,³⁸ suggesting the presence of Pd and Ag atoms in a zero-valent state for these three samples.

We demonstrated the use of 2,6-DMPI as a sensitive probe to characterize the outermost layer of concave surfaces for Ag-Pd nanocrystals by SERS. Because the lone pair of electrons would bind to Ag and Pd through σ -donation and π -back-donation, respectively, we can simply follow the change in the vibration frequency of NC bond (ν_{NC}) to monitor the deposition of Pd on Ag nanocrystals.³⁹ Figure 6 shows the SERS spectra of 2,6-DMPI adsorbed onto the Ag nanocubes before and after they had reacted with different volumes of the Pd(II) precursor solution. Before the introduction of the Pd(II) precursor, the characteristic peak located at 2179 cm^{-1} could be assigned to the NC stretching band of 2,6-DMPI, $\nu_{\text{NC(Ag)}}$.⁴⁰ At 0.05 mL, we observed the decrease in peak intensity for the $\nu_{\text{NC(Ag)}}$ peak while a new peak emerged at 2108 cm^{-1} , with its assignment to the $\nu_{\text{NC(Pd)}}$ band.⁴¹ Although it is difficult to rely on TEM imaging to identify Pd atoms being deposited on the Ag nanocubes (see Figure 1A), this result indicated that the outermost surface,

likely on the edges of nanocubes where the SERS hot spots are located, was composed of both newly deposited Pd atoms and the remaining Ag atoms. At 0.1 mL, the $\nu_{\text{NC(Pd)}}$ peak became dominant in terms of intensity while the $\nu_{\text{NC(Ag)}}$ band became a shoulder peak, confirming the predominant coverage of Pd atoms on the outermost layer of concave surfaces where SERS signal was collected. We also noticed the decrease in SERS intensity. With a further increase in the volume of the Pd(II) precursor solution to 0.2 and 0.4 mL, we could only resolve the $\nu_{\text{NC(Pd)}}$ band but not the $\nu_{\text{NC(Ag)}}$ peak, together with a continuing decrease in SERS intensity. Although the SERS hot spots could still be created on the concave nanocrystals to promote a stronger SERS activity, the deposition of Pd would coincide with these hot spots for alleviating signal tremendously due to the weak coupling between the conduction electrons of Pd and visible light.^{42,43} Taken together, we argue that Pd atoms would become predominant at the outermost layer of the concave surface prepared with 0.1 mL of the precursor solution and beyond.

Conclusions

We have demonstrated the transformation of Ag nanocubes into Ag-Pd concave nanocrystals by introducing the Pd(II) precursor solution into an aqueous suspension of Ag nanocubes in the presence of CTAC under ambient conditions. When Cl^- ions derived from CTAC was involved in the reaction system, we identified the carving of Ag atoms on the side faces of nanocubes through oxidation while Pd atoms derived from the reduction of Pd(II) precursor by Ag would be deposited on the edges of nanocubes. In turn, we rely on a simple galvanic replacement reaction to reproducibly generate Ag-Pd concave nanocrystals with the ability to control the Pd content from 0.4 wt.% to 2.8 wt.%. By using an isocyanide molecule as a sensitive probe, we examined the outermost layer of concave surfaces for the as-obtained Ag-Pd nanocrystals by SERS, confirming the presence of Pd atoms on these concave surfaces where SERS hotspots are located. We believe that this methodology would become useful to synthesize Ag-based concave nanostructures with other metal such as Pt, Rh, and Ir.

Supporting Information

Figures S1-S7 and Tables S1-S3 are provided in the Supporting Information (SI).

Acknowledgement

We acknowledge the support from the National Science Foundation (CHE-1708300) and start-up funds from the Georgia Institute of Technology (GT). We also acknowledge the use of the materials characterization facilities at the Institute of Electronics and Nanotechnology at GT.

Notes and References

- 1 M. Rycenga, C. M. Cobley, J. Zeng, W. Li, C. H. Moran, Q. Zhang, D. Qin, Y. Xia, *Chem. Rev.* **2011**, *111*, 3669–3712.
- 2 K. A. Willets and R. P. Van Duyne, *Annu. Rev. Phys. Chem.*, 2007, **58**, 267–297.
- 3 A. J. Haes, C. L. Haynes, A. D. McFarland, G. C. Schatz, R. P. Van Duyne and S. Zou, *MRS Bull.*, 2005, **30**, 368–375.
- 4 P. K. Jain, X. Huang, I. H. El-Sayed and M. A. El-Sayed, *Acc. Chem. Res.*, 2008, **41**, 1578–1586.
- 5 J. P. Camden, J. A. Dieringer, J. Zhao and R. P. Van Duyne, *Acc. Chem. Res.*, 2008, **41**, 1653–1661.
- 6 M. R. Jones, K. D. Osberg, R. J. Macfarlane, M. R. Langille and C. A. Mirkin, *Chem. Rev.*, 2011, **111**, 3736–3827.
- 7 C. Gao, Z. Lu, Y. Liu, Q. Zhang, M. Chi, Q. Cheng, and Y. Yin, *Angew. Chem. Int. Ed.* 2012, *57*, 5629–5633.
- 8 S. Nie and S. R. Emory, *Science*, 1997, **275**, 1102–1106.
- 9 J. P. Camden, J. A. Dieringer, Y. Wang, D. J. Masiello, L. D. Marks, G. C. Schatz and R. P. Van Duyne, *J. Am. Chem. Soc.*, 2008, **130**, 12616–12617.
- 10 A. M. Michaels, M. Nirmal and L. E. Brus. *J. Am. Chem. Soc.*, 1999, **121**, 9932–9939.
- 11 A. B. Zrimsek, N. Chiang, M. Mattei, S. Zaleski, M. McAnally, C. Chapman, A.-I. Henry, G. C. Schatz and R. P. Van Duyne, *Chem. Rev.*, **2017**, *117*, 7583–7613.
- 12 A. B. Zrimsek, N. Wong and R. P. Van Duyne, *J. Phys. Chem. C*, 2016, **120**, 5133–5142.
- 13 P. Christopher, H. L. Xin and S. Linic, *Nat. Chem.*, 2011, **3**, 467–472.
- 14 P. Christopher and S. Linic, *J. Am. Chem. Soc.*, 2008, **130**, 11264–11265.
- 15 J. Li, Y. Wu, X. Sun, J. Liu, S. A. Winget and D. Qin, *ChemNanoMat*, 2016, **2**, 786–790.
- 16 Y. Wu, X. Sun, Y. Yang, J. Li and D. Qin, *Acc. Chem. Res.*, 2017, **50**, 1774–1784.
- 17 Y. Zhang, Y. Wu, and D. Qin, *J. Mater. Chem. C*, 2018, **6**, 5353–5362.

- 18 J. Chen, B. Wiley, J. Mclellan, Y. Xiong, Z. Y. Li and Y. Xia, *Nano Lett.*, 2005, **5**, 2058–2062.
- 19 M. A. Mahmoud and M. A. El-Sayed, *Langmuir*, 2012, **28**, 4051–4059.
- 20 A. N. Chen, S. M. McClain, S. D. House, J. C. Yang, and S. E. Srabalak, DOI: 10.1021/acs.chemmater.8b04630.
- 21 H. Jing and H. Wang, *Chem. Mater.*, 2015, **27**, 2172–2180.
- 22 J. Li, J. Liu, Y. Yang and D. Qin, *J. Am. Chem. Soc.*, 2015, **137**, 7039–7042.
- 23 J. Li, X. Sun and D. Qin, *ChemNanoMat*, 2016, **2**, 494–499.
- 24 H. Zhang, M. J. and Y. Xia, *Angew. Chem., Int. Ed.* 2012, **51**, 7656–7673.
- 25 X. Xia, J. Zeng, B. Mcdearmon, Y. Zheng, Q. Li and Y. Xia, *Angew. Chem., Int. Ed.* 2011, **123**, 12750–12754.
- 26 B. Jiang, L. Xu, W. Chen, C. Zou, Y. Yang, Y. Fu and S. Huang, *Nano Res.* 2017, **10**, 3509–3521.
- 27 Q. Zhang, Y. Zhou, E. Villarreal, Y. Lin, S. Zou and H. Wang, *Nano Lett.* 2015, **15**, 4161–4169.
- 28 J. Zhang, M. R. Langille, M. L. Personick, K. Zhang, S. Li and C. A. Mirkin, *J. Am. Chem. Soc.* 2010, **132**, 14012–14014.
- 29 T. Yu, D. Y. Kim, H. Zhang and Y. Xia, *Angew. Chem., Int. Ed.* 2011, **123**, 2825–2829.
- 30 M. Jin, H. Zhang, Z. Xie and Y. Xia, *Angew. Chem., Int. Ed.* 2011, **123**, 7996–8000.
- 31 S. Zhou, J. Ki, K. D. Gilroy, J. Tao, C. Zhu, X. Yang, X. Sun and Y. Xia, *ACS Nano*, 2016, **10**, 9861–9870.
- 32 J. Du, Z. Chen, C. Chen and T. J. Meyer, *J. Am. Chem. Soc.*, 2015, **137**, 3193–3196.
- 33 K. Mech, P. Zabinski, R. Kowalik and K. J. Fitzner, *Electrochem. Soc.*, 2013, **160**, H770–H774.
- 34 Q. Zhang, W. Li, L. P. Wen, J. Chen and Y. Xia, *Chem. Eur. J.*, 2010, **16**, 10234–10239.
- 35 L. I. Elding, L. F. Oisson, *J. Phys. Chem.*, 1978, **82**, 69–74.
- 36 C. Colombo, C. J. Oates, A. J. Monhemius and J. A. Plant, *Geochem.: Explor., Environ., Anal.*, 2008, **8**, 91–101.
- 37 J. Ahn, D. Wang, Y. Ding, J. Zhang and D. Qin, *ACS Nano*, 2018, **12**, 298–307.
- 38 J. F. Moulder, W. F. Stickle, P. E. Sobol, K. D. Bomben, Handbook of X-ray Photoelectron Spectroscopy, Perkin–Elmer Corporation, *Physical Electronics Division*, **1992**.
- 39 Y. Wu and D. Qin, *J. Am. Chem. Soc.*, 2018, **140**, 8340–8349.

- 40 S. J. Bae, C. Lee, I. S. Choi, C.-S. Hwang, M.-S. Gong, K. Kim and S.-W. Joo, *J. Phys. Chem. B*, 2002, **106**, 7076–7080.
- 41 K. Kim, K. L. Kim, J. Y. Choi, H. B. Lee and K. S. Shin, *J. Phys. Chem. C*, 2010, **114**, 3448–
- 42 Y. Zhang, X. Gao and M. J. Weaver, *J. Phys. Chem.*, 1993, **97**, 8656–8663.
- 43 J. M. McLellan, Y. Xiong, M. Hu and Y. Xia, *Chem. Phys. Lett.*, 2006, **417**, 230–234.

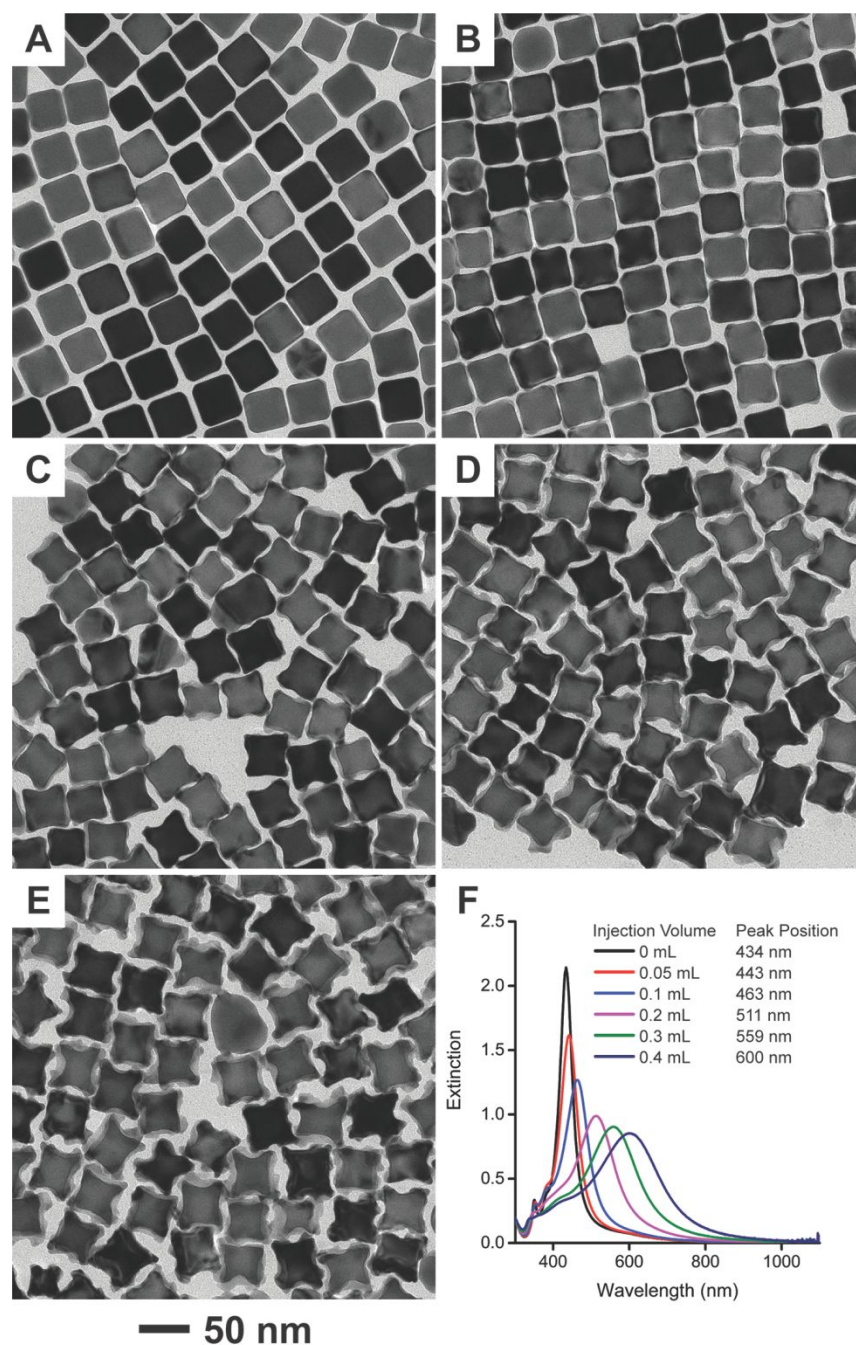


Figure 1. TEM images of concave nanocrystals prepared by reacting Ag nanocubes with different volumes of the Pd(II) precursor solution: (A) 0.05 mL, (B) 0.1 mL, (C) 0.2 mL, (D) 0.3 mL, and (E) 0.4 mL, respectively, in the presence of CTAC. (F) UV-vis spectra of Ag nanocubes before and after reacting with different volumes of the Pd(II) precursor solution.

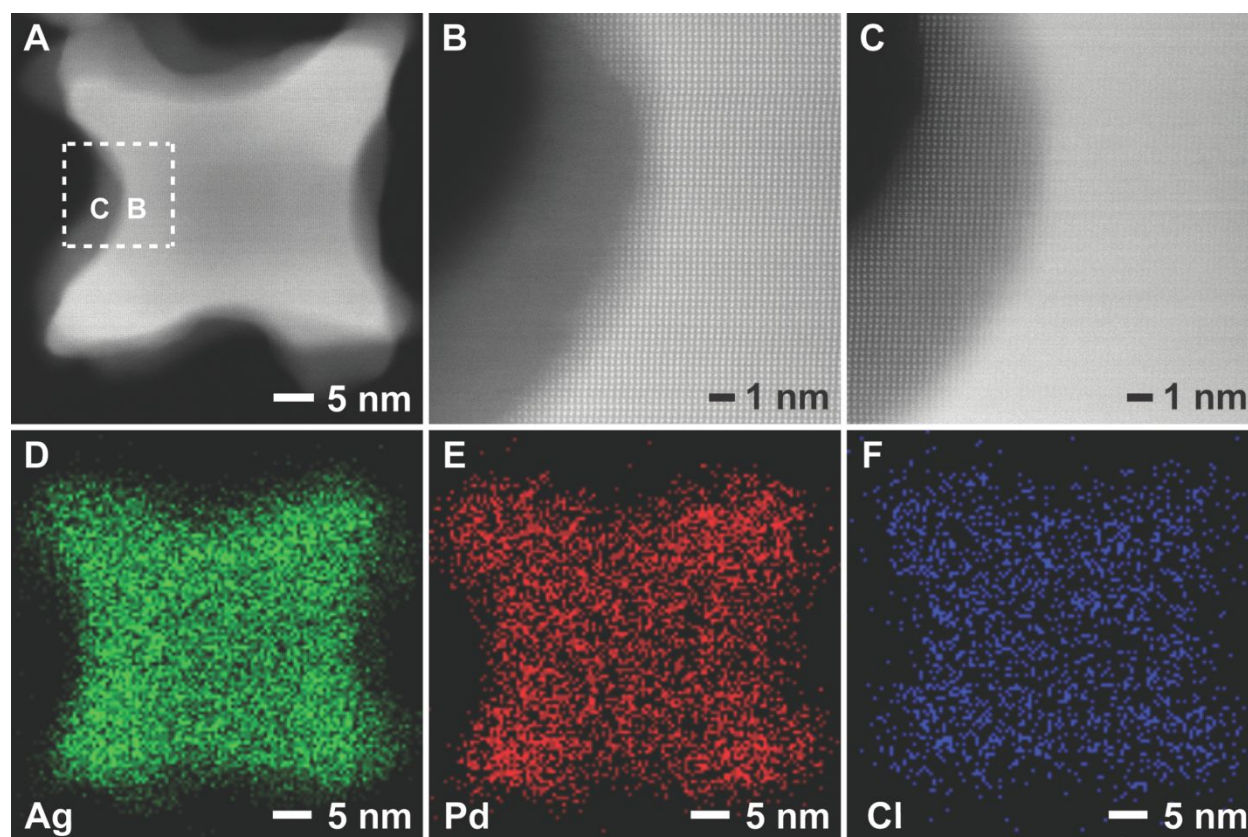


Figure 2. (A-C) HAADF-STEM images of a sample prepared with the addition of 0.4 mL of the Pd(II) precursor solution (see Figure 2E). (D-F) EDX elemental mapping of the same sample (green: Ag; red: Pd; blue: Cl).

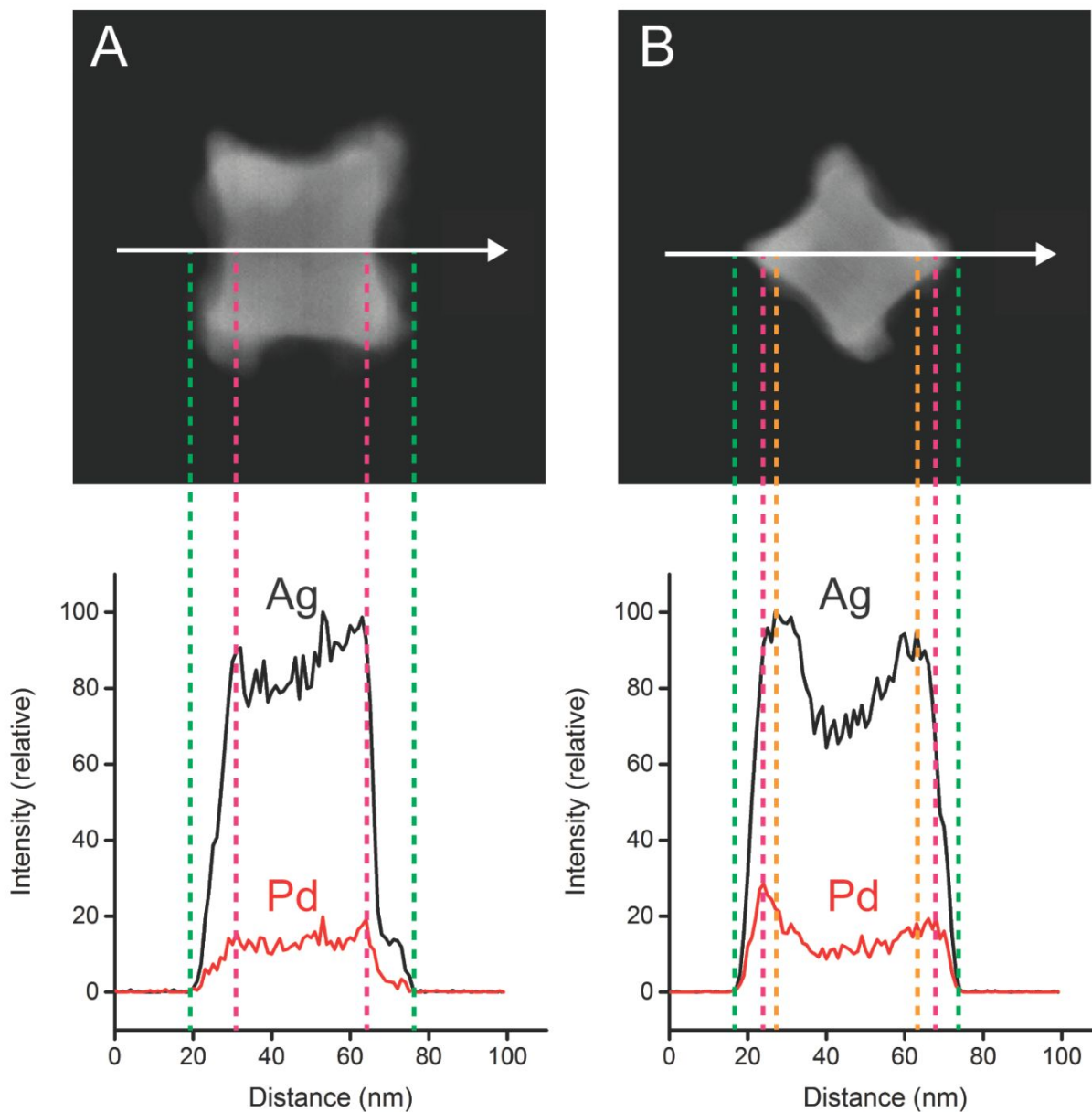


Figure 3. (A) A HAADF-STEM image taken from an individual concave nanocrystal prepared with 0.4 mL of the Pd(II) precursor solution and the corresponding EDS line-scan results. (B) A HAADF-STEM image taken from the same particle in (A) but with the raster angle rotated by 45 degrees and the corresponding EDS line-scan data. The particle was oriented along the $\langle 001 \rangle$ zone axis.

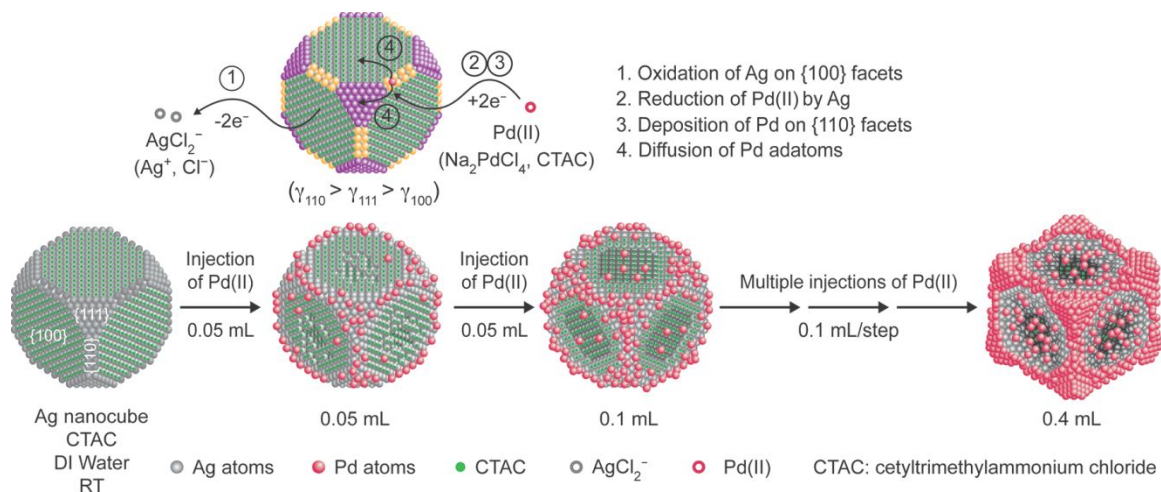


Figure 4. (top) Schematic illustration of proposed mechanism accounted for the oxidation of Ag on the {100} facets of a CTAC-capped Ag nanocube, the reduction of Pd(II) by Ag to generate Pd atoms for their deposition on the {110} facets, and the diffusion of Pd adatoms across the surface. (bottom) Illustration of the transformation of a Ag nanocube into a Ag-Pd nanocube and two subsequent concave nanocrystals with different concavities on the side faces of nanocubes with different volumes of Pd(II) precursor in the presence of CTAC.

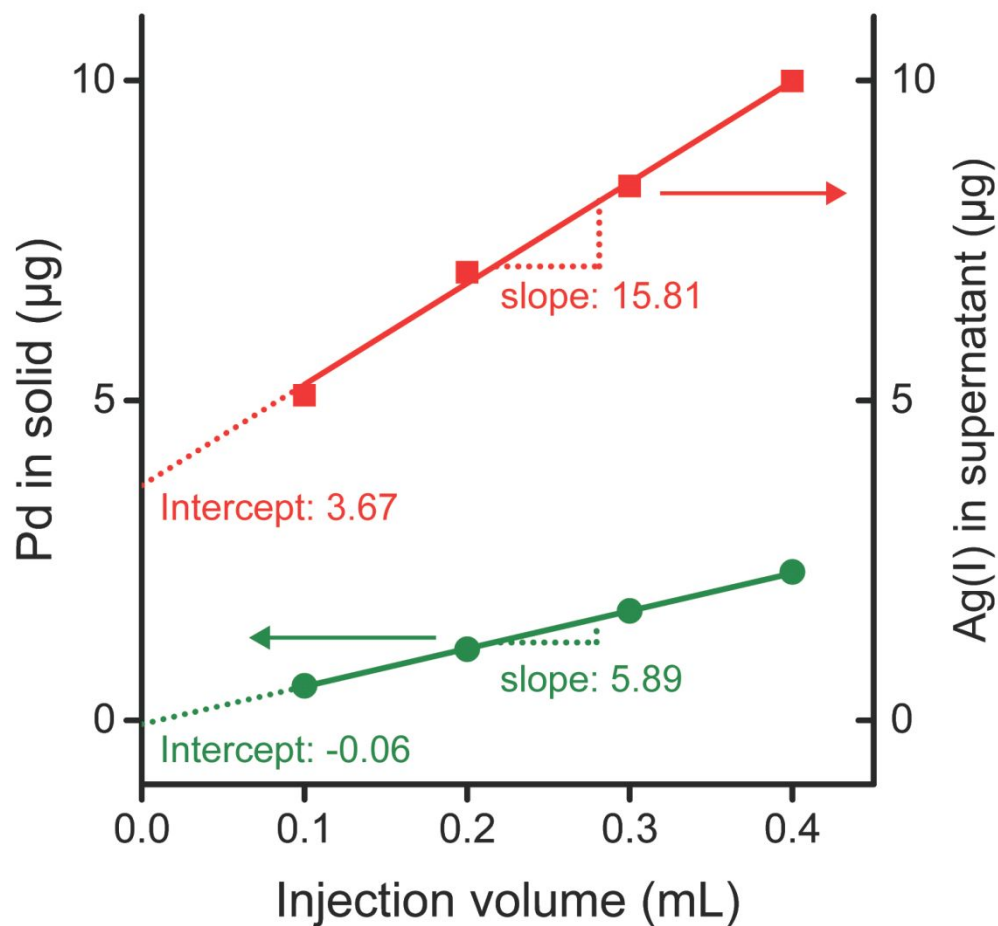


Figure 5. ICP-MS data of Pd in solids and Ag(I) in supernatant for the corresponding products prepared by introducing different volumes of the Pd (II) precursor solution into an aqueous suspension of Ag nanocubes in the presence of CTAC.

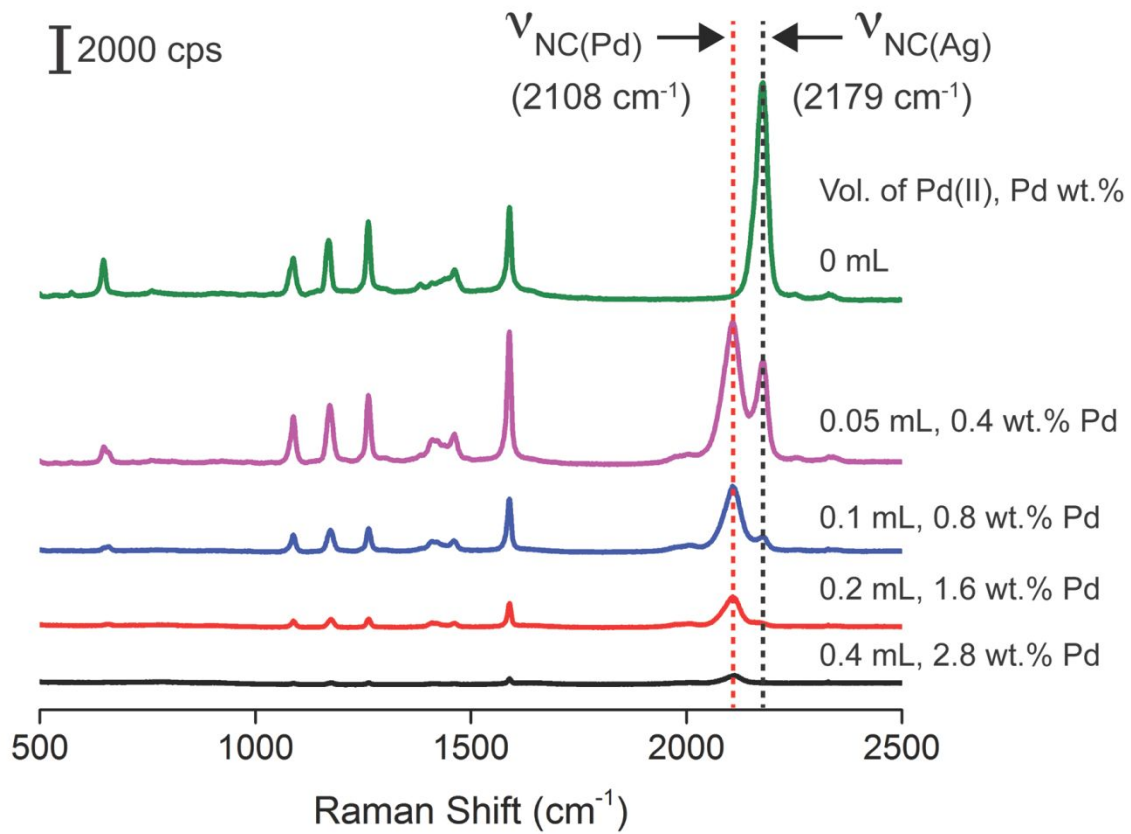


Figure 6. SERS spectra recorded from the CTAC-treated, 2,6-DMPI-functionalized Ag nanocubes and the Ag-Pd nanocrystals prepared with different volumes of the Pd(II) precursor solution.